

Extending the operation of a solar air collector to night-time by integrating radiative sky cooling: a comparative experimental study

Mingke Hu [a], Bin Zhao [b], Suhendri [a], Jingyu Cao [c], Qiliang Wang [d], Saffa Riffat [a], Yuehong Su [a, *], Gang Pei [b, *]

[a] *Department of Architecture and Built Environment, University of Nottingham, University Park, Nottingham NG7 2RD, UK*

[b] *Department of Thermal Science and Energy Engineering, University of Science and Technology of China, Hefei 230027, China*

[c] *College of Civil Engineering, Hunan University, Changsha 410082, China*

[d] *Department of Building Services Engineering, The Hong Kong Polytechnic University, Kowloon, Hong Kong, China*

---

* Corresponding author: yuehong.su@nottingham.ac.uk; peigang@ustc.edu.cn

Abstract

Solar thermal collectors are generally unproductivity at night without sunlight. Radiative cooling, on the other hand, is another renewable technology harvesting coldness from extraterrestrial space and can effectively work nocturnally. Therefore, this study proposes a scheme that integrates the nocturnal radiative cooling mechanism into a solar air collector as a supplementary. Incoming air is heated by the solar absorber during the daytime and cooled down by the glass cover at night. Experimental results indicate that, with an air mass flow rate of 0.03kg/s, the dual-mode collector (named as PT-RC collector) realized a daytime solar thermal efficiency of 34.2% at zero-reduced temperature (e.g., when the inlet air temperature equals the ambient temperature) and a net radiative cooling power (e.g., when the inlet air temperature equals the ambient temperature) of 27.9 W/m^2, which are 72.2% and 2.4 times those of the typical solar air collector. As the air mass flow rate increased from 0.01 to 0.05kg/s, the two

performance indicators lifted from 19.8% to 34.5% and from 16.9 to 33.0 W/m^2, respectively. The PT-RC collector shows potential to be applied in four-season regions where heating and cooling are both required throughout the year or tropical zones where cooling is much more desired.

Keywords: *solar energy; solar air collector; radiative cooling; dual-mode; thermal efficiency; cooling power.*

1. Introduction

Current energy and environment dilemmas call for revolution from the energy supply-side [1]. Solar energy, as a clean and sustainable energy source, plays an increasing role in this context [2]. The sun (~5800 K) constantly emits enormous energy, of which approximately1.8×10^{14} kW reaches the earth's surface [3]. Though most incident solar radiation is dissipated into heat spontaneously, the energy density is too low to heat an object up to a temperature significantly higher than the ambient temperature. Various solar-thermal conversion technologies, therefore, have been introduced and developed to boost the solar heating effect and get high-temperature heat sources [4-6]. Flat-plate solar thermal collectors are the most well-developed among different solar thermal installations, which have been widely employed for building energy-saving [7], crop drying [8], water desalination [9], etc. Water and air are two natural working fluids widely used as thermal carriers in flat-plate solar thermal collectors [10, 11]. While the thermal efficiency of an air-based solar collector is generally lower than that of a water-based one, it owns superiorities in terms of structure simplicity [12], low cost [13], freezing-free [14], etc. Therefore, solar air heaters are commonly applied in fields such as the building and agriculture sectors to provide hot air for space heating [15] and drying application [16] directly. For example, the solar air collector can be deployed on the sun-facing façade (also named as "Trombe wall" in some cases [17]) and roof to increase the indoor air temperature on cold sunny days.

Typically, a solar thermal collector is equipped with a solar selective absorbing coating on the solar absorber to maximize the thermal efficiency. However, as current available SSACs are spectrally-static (extremely high solar absorptivity and low long-wave emissivity [18]), a solar thermal collector can only and will always absorb solar energy and convert it into heat when exposed to sunlight. As a consequence, the building-integrated solar air collector/system has two inherent shortcomings in regulating the indoor thermal environment. First, the solar air collector usually cannot run at night due to the absence of solar radiation [19]. This unoccupancy prolongs the payback period of the system. Second, given that the heating and cooling demands in buildings vary through the year in most regions across the world, a solar thermal collector shows poor seasonal and regional flexibility when applied to the building sector as a mono-function device. That is to say, a solar thermal collector may suffer from inefficacy in hot seasons [20]. Moreover, some types of building-integrated solar collectors (e.g., the Trombe wall [21]) may even create an undesired heating effect in summer and thus increase the building cooling load. If the solar thermal collector could act as a cooler when cooling energy is needed, its seasonal and regional adaptability will be significantly improved to match the building energy demands better. Nocturnal radiative cooling can exactly meet this purpose by throwing waste heat into the cold sky through the primary "atmospheric window" in 8 to 13 μm [22].

Radiative sky cooling is considered another renewable energy technology which has drawn wide attention in recent years [23]. Generally, to achieve remarkable cooling performance, a radiative cooler should exhibit high spectral emissivity in the "atmospheric window", allowing it to strongly emit thermal energy to the extraterrestrial space [24]. The spectral emissivity (i.e., spectral absorptivity) outside the "atmospheric window", on the other hand, should be as low as possible, aiming for creating a larger ambient-emitter temperature gap [25]. In particular, the emitter requires an extraordinarily high spectral reflectivity in the solar radiation band (0.2 to 3 μm), provided daytime radiative cooling is pursued [26]. However, the spectral requirement tends to be much looser if a radiative emitter only needs to operate at night. A nocturnal radiative cooler not necessarily needs to show rigid spectral selectivity from ultraviolet to far-infrared bands only if it exhibits high emissivity in the "atmospheric window". In fact, a greater radiative cooling power will be achieved if the emitter has high emissivity throughout the infrared band [27]. This makes such materials as black paint [28] and silicon dioxide [29] perform good nocturnal radiative cooling.

Therefore, if a solar thermal collector could run as a nocturnal radiative cooler, its operation period could be extended and its seasonal and regional adaptability would be enhanced. The integration of solar heating and radiative cooling into a single collector can be tracked back to the 1980s when Matsuta et al. [30] firstly proposed a solar photothermic and radiative cooling (PT-RC) collector employing water as the working medium. A spectrally selective surface was equipped in the PT-RC collector and acted as a solar absorber during the daytime and as a radiative emitter during the nighttime. Pei's group further developed this spectrally selective PT-RC technology [31]. They prepared a PT-RC coating consisting of an aluminium substrate, a middle layer of solar selective absorbing coating, and a top layer of polyethylene terephthalate, based on which the PT-RC collector realized a diurnal PT efficiency of 62.7% at zero-reduced temperature and a nocturnal net RC flux of 50.3 W/m^2. They further designed an advanced PT-RC coating consisting of a layer of polydimethylsiloxane, two layers of Ni-Al_2O_3 mixing material [32]. Desired spectral characteristics enable the coating to be heated to 79.1 °C above the ambient temperature during the daytime and be cooled to 10 °C below the ambient temperature at night. Noticing that the diurnal solar heating performance of the spectrally selective PT-RC collector is lower than that of the typical solar thermal collector, Janus and rotary PT-RC collectors with one surface acting as the solar absorber and the opposite or adjacent surface being the radiative cooler have also been proposed to minimize the penalty on solar thermal performance [33-35].

While the water-based PT-RC collector has been widely investigated, the one using air as the thermal carrier has not yet received much attention. However, due to the relatively low radiative cooling power and high heat capacity of the water, the inlet-outlet water temperature difference is very small, which means the water may need to be circulated before reaching a low enough temperature. In contrast, with much lower heat capacity, the airflow passing through an air-based PT-RC collector may be able to reach a sufficient sub-ambient temperature and be sent to the end-user directly. Given that the glass cover in a solar air collector is mainly composed of silicon dioxide and shows very high long-wave emissivity, it is possible to take it as a nocturnal radiative cooling emitter, by which way we can integrate the radiative cooling scheme into the solar air collector and extend the operation to nighttime. Therefore, in this work, we propose a new dual-mode collector slightly adjusted from a flat-plate solar air collector for the purpose of realizing daytime solar heating and nighttime radiative cooling. The new module, named as air-based solar photothermic and radiative cooling (PT-RC) collector, is expected to deliver heat during cold daytime and coldness during hot nighttime in tune with the energy demands in buildings. A prototype air-based dual-mode PT-RC collector and a typical flat-plate solar air collector were designed and fabricated before being tested on an outdoor experimental platform. The thermal performance of the air-based dual-mode PT-RC collector and typical solar air collector in different working conditions was investigated and compared in this study.

2. Description of the air-based PT-RC collector and experimental setup

2.1. Air-based PT-RC collector

Fig. 1(B) illustrates the cross-section schematic diagram of the air-based PT-RC collector. As a comparison, that of a typical flat-plate solar air collector is shown in Fig. 1(A). The aperture area of the two collectors is 1.89 m^2 (1960 mm * 964 mm). The air-based PT-RC collector comprises a low-density polyethylene (PE) film, a glass cover, a solar absorber, a thermal insulation layer, and frames. The PE film is set on top of the glass cover with a 40 mm-height air gap between them to limit the heat exchange between the glass cover and ambient air (especially at night). High spectral transmittance in both solar spectrum and infrared wavelengths of the PE film allows solar radiation and glass thermal emission to pass through it freely. The glass cover shows high solar transmittance but high emissivity in the rest band, making it a suitable nighttime radiative emitter. Therefore, the glass cover will strongly emit thermal energy to the cold sky through the transparent PE cover and "atmospheric window" and reach a sub-ambient temperature during the nighttime without solar irradiation. The solar absorber is deposited with a spectral selective absorbing coating which shows strong solar absorption but weak thermal emission. With a thickness of 50 mm, the thermal insulation layer is arranged beneath the solar absorber to minimize the backward thermal loss of the collector. A 30 mm-height air duct is arranged between the glass cover and solar absorber, allowing the incoming airflow to extract heat from the absorber in diurnal solar heating mode and transfer heat to the glass cover in nocturnal radiative cooling mode. In contrast, the air duct in the typical solar air collector, with the same height of 30 mm, is set between the solar absorber and thermal insulation layer, which is the most common structure among various solar air collectors.

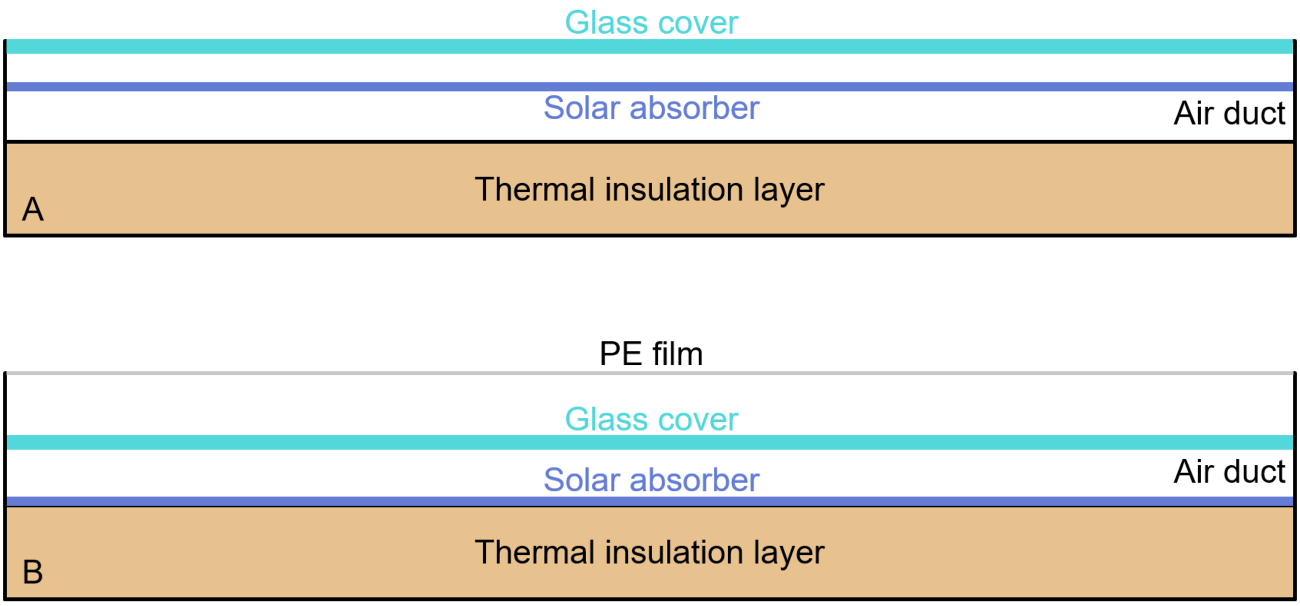

Fig. 1. The cross-section schematic diagram of the (A) typical solar air collector and (B) air-based PT-RC collector.

2.2. Experimental setup

To test the thermal performance of the air-based PT-RC collector, an outdoor experimental testing platform was set up on the rooftop of a building in the University of Science and Technology of China, Hefei. As shown in Figs. 2 and 3, the testing system mainly includes an air-based PT-RC collector, a typical solar air collector, an air handling unit, connecting air pipes, several measuring sensors (for temperatures, solar irradiance, wind velocity, air mass flow rate, etc.), and a data logger.

To conduct performance comparisons of the air-based PT-RC collector and the typical solar air collector, the specifications and settings relevant to the two collectors are the same, including the collector area (1.89 m^2), inclinations angle (30°), and orientation (due south), measuring sensors and their locations relative to the collector, inlet air temperature and mass flow rate, etc. The air handling unit as a whole is a moveable cabinet including several chambers. The ambient air was employed as the thermal carrier during the test, being sucked into the air handling unit through the air inlet (with a dust filter) on one side of the cabinet and then passing through the two air collectors and finally flowing back to the ambient through the air out on another side of the cabinet. An air conditioner was integrated into the cabinet to firstly cool and dehumidify the ambient air. After that, the air flows to the air heating chamber and is heated by the heating wires evenly. The cooling power provided by the air conditioner is fixed while the heating power provided by the heating wire can be steplessly regulated. Therefore, the air temperature at the inlet of the two collectors can be controlled flexibly. The connecting air pipe between the air handling unit and the inlet of the two collectors were thermally well-insulated to minimize external thermal interference. Four platinum resistances (PT 100, four-wired, ±0.1 °C) were respectively inserted at the inlet and outlet of the two collectors to measure the air temperatures. Two air valves were installed in the connecting air pipe between the air handling unit and the outlet of the two collectors to adjust the air mass flow rate during the experiments. As shown in the right-top part of the cabinet is the air mass flow rate measuring unit which mainly includes two nozzle sets, two platinum resistances, four air pressure sensors, two differential pressure transmitters, and four air diffuser plates. Following the guideline of GB-T 17758-2010, the air mass flow rate is measured according to the nozzle specification, air temperature and pressure at the inlet of the nozzle, and the air pressure difference between the inlet and outlet of the nozzle. At the right-bottom of the cabinet in Fig. 2 is an air blower which drives the air stream to the ambient. Several thermocouples (Type T, ± 0.5 °C) are arranged on the lower surface of the solar absorber to measure the absorber temperatures. Another thermocouple is placed in a thermometer shelter nearby to measure the ambient temperature. A pyranometer (TBQ-2A, ±2%) with the same inclination angle as the collector is arranged to monitor the solar irradiance. An anemometer (HSTL-FS01, ±0.2 m/s) is placed on the support to record the ambient wind velocity. All measured data are recorded by the data logger (HIOKI LR8450) placed in the cabinet of the air handling unit. During each test, the system operated in advance for a short period to reach the quasi-steady-state, and after that the data recorded by the data logger were adopted for analysis. The experimental testing and monitoring instruments and their uncertainties are listed in Table 1.

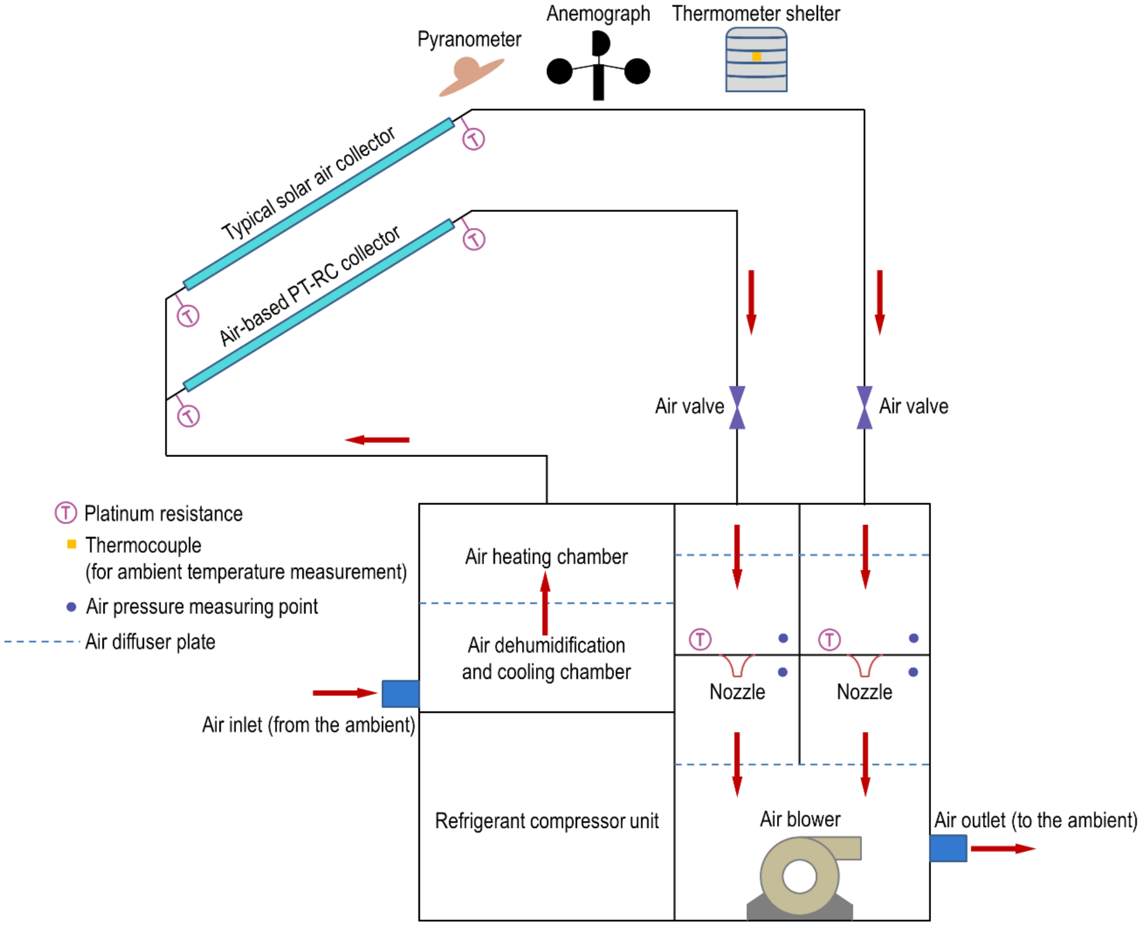

Fig. 2. Schematic of the experimental testing system.

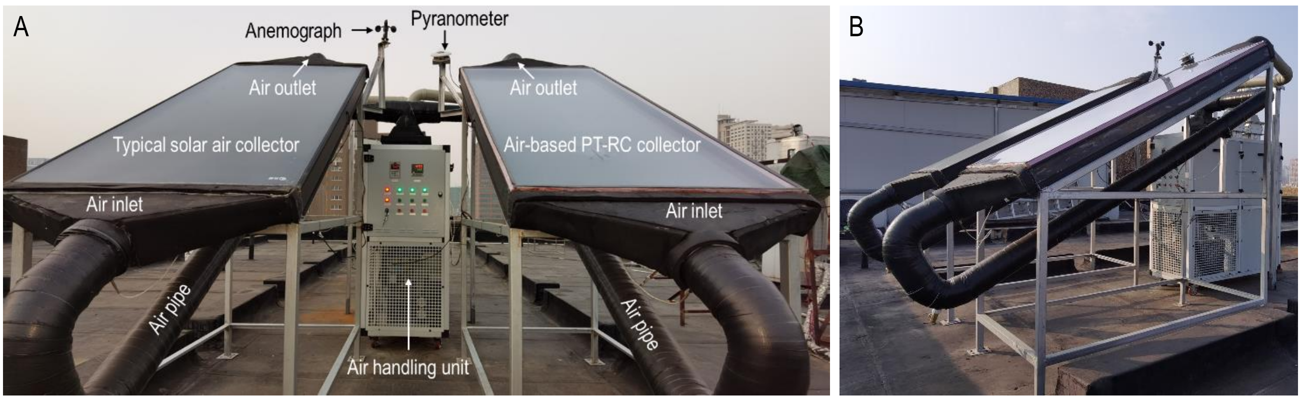

Fig. 3. In-situ photos of the experimental testing system. (A) front view, and (B) side view.

Table 1. List of main testing and monitoring devices in the experimental system.

Device	Specification	Uncertainty

Pyranometer	TBQ-2A	±2%
Anemograph	HSTL-FS01	±0.2 m/s
Pressure sensor	/	±0.25%
Differential pressure transmitter	Yokogawa-EJA	±0.1%
Platinum resistance	OMEGA-PT100	±(0.03+0.001| t |) °C
Thermocouple	Type T (copper-constantan)	±0.5 °C
Data logger	HIOKI LR8450	/

3. Performance evaluation model and experimental method

3.1. Performance evaluation model

The air-based PT-RC collector can operate in two modes, namely, daytime solar heating mode and nighttime radiative cooling mode. The solar thermal efficiency of the collector is employed as the performance indicator in the daytime solar heating mode, and the cooling power of the collector is used as the evaluator in the nighttime radiative cooling mode.

3.1.1 Daytime solar heating mode

In the daytime solar heating mode, the solar thermal efficiency of the collector is defined as the heat gain of the air stream flow along the air duct divided by the incident solar energy, with the expression written as follows:

$$\eta_{\mathrm{th}} = \frac{Q_{\mathrm{he}}}{H_{\mathrm{s}}} = \frac{\dot{m} c_{\mathrm{a}} \left(T_{\mathrm{out}} - T_{\mathrm{in}} \right)}{G A_{\mathrm{c}}} \tag{1}$$

where Q_{he} is heat gain of the air stream, J/s; H_s is the incident solar radiation, J/s; $\dot{m}$ is the mass flow rate of the airflow, kg/s; c_a is the specific heat capacity of water, J/(kg·K); T_{in} and T_{out} are respectively the air temperature at the inlet and outlet of the collector, K; G is the solar irradiance, W/m^2; and A_c is the aperture area of the collector, m^2.

The mass flow rate of the airflow is calculated by:

$$\dot{m} = 1.414 C A_{\mathrm{n}} \left(p_{\mathrm{v}} V_{\mathrm{in}}{}' \right)^{0.5} \tag{2}$$

$$V_{\mathrm{n}}' = \frac{p_0 V_{\mathrm{n}}}{\left[\left(1+W_{\mathrm{n}}\right) p_{\mathrm{n}}\right]} \tag{3}$$

where C is flow coefficient and is 0.98 in this study; A_{n} is the throat area of the nozzle, m^2; p_{v} is the static pressure difference between the inlet and outlet of the nozzle, pa; p_{n}, and p_0 are respectively the air pressure at the inlet and local ambient, Pa; V_{n}' is the specific volume of the air at the inlet of the nozzle, m^3/kg; V_{n} is the specific volume of the air at the inlet of the nozzle in the standard atmosphere condition, m^3/kg; W_{n} is the moisture content of the air at the inlet of the nozzle and is 0 in this study.

3.1.2. Nighttime radiative cooling mode

In the nighttime radiative cooling mode, the cooling power of the collector is defined as the heat loss of the air stream passing through the collector divided by the area of the collector, expressed as follows:

$$P_{\mathrm{co}} = \frac{Q_{\mathrm{co}}}{A_{\mathrm{c}}} = \frac{\dot{m} c_{\mathrm{a}} \left(T_{\mathrm{in}} - T_{\mathrm{out}}\right)}{A_{\mathrm{c}}} \tag{4}$$

where Q_{co} is the cooling gain of the air stream, J/s.

The measuring error of the solar thermal efficiency cooling power of the collector can be determined based on error propagation theory. In specific, the relative error (*RE*) of a dependent variable y can be expressed as:

$$RE_y = \frac{dy}{y} = \left|\frac{\partial f}{\partial x_1}\right| \frac{\Delta x_1}{y} + \left|\frac{\partial f}{\partial x_2}\right| \frac{\Delta x_2}{y} + \cdots + \left|\frac{\partial f}{\partial x_n}\right| \frac{\Delta x_n}{y} \tag{5}$$

$$y = f(x_1, x_2, \cdots, x_n) \tag{6}$$

where x_{i}, (i = 1, …, n) is the independent variable of y, $\partial f / \partial x$ is the error transferring coefficient of the variables, and Δx_{i} is the measuring error of the independent variable.

The experimental relative mean error (*RME*) of a dependent variable y during the test can be calculated by:

$$RME_y = \frac{\sum_1^N RE_y}{N} \tag{7}$$

where N is the number of measuring data.

3.2. Experimental method

To comprehensively characterize the thermal performance of the air-based PT-RC collector and compare it with that of the typical solar air heater, the two collectors were operated and tested in different working conditions. In specific, consecutive daytime solar heating and nighttime radiative cooling performance at constant air mass flow rate and near-ambient inlet temperature were investigated on several days firstly. The effect of inlet air temperature and mass flow rate on the thermal performance of the collector was also studied by regulating the air heating power and valve opening in the air handling unit.

4. Results and discussion

4.1. Consecutive daytime solar heating and nighttime radiative cooling

Firstly, the daytime solar heating and nighttime radiative cooling performance of the air-based PT-RC collector and the typical solar air collector (hereafter referred to as “PT-RC collector” and “PT collector” for better comparisons in Section 4) was tested continuously from 08:00, Nov 2nd to 16:00, Nov 3rd, 2020, and the results are shown in Fig. 4. The air mass flow rate of the two collectors stayed at about 0.03 kg/s during the test, and the ambient air was directly fed to the inlet of the two collectors without the pre-heating and/or cooling process. Hence, the inlet air temperatures were quite close to that of the ambient temperature, especially during the nighttime (the temperature gap during the daytime is mainly due to the extra heat absorption of the air stream in the air pipe which was heated up under sunlight exposure). With almost the same inlet air temperatures, the PT and PT-RC collectors show distinctly different outlet air temperatures during the daytime, particularly around noon-time with intensive solar radiation, indicating that the PT collector shows better solar thermal performance. In specific, the maximum inlet-outlet air temperature difference of the PT collector reached 26.9 °C, which is about 7.9 °C higher than that of the PT-RC collector. This is mainly caused by the structural differences between the two collectors. The air duct in the PT collector is set between the solar absorber and thermal insulation layer, while that in the PT-RC collector is positioned between the solar absorber and glass cover. Therefore, the convective heat exchange between the absorber and glass cover in the PT-RC collector is significantly greater than that in the PT collector when the air in the air duct flows. As a result, the glass cover in the PT-RC collector reaches a much higher temperature and dissipates much more heat to the ambient through thermal radiation. Previous studies have also proved that the former air duct structure shows higher thermal efficiency than the latter for the flat-plate solar air heater [36, 37]. In addition, although the PE film atop the glass cover shows very high solar transmittance, it partially decreases the solar irradiance projected on the solar absorber of the PT-RC collector and thus further degrades the solar thermal efficiency. As suggested in Table 2, the average thermal efficiency of the PT-RC collector during the solar heating mode (08:00 to 16:00) was 33.1%, which is around 70% of that of the typical PT collector.

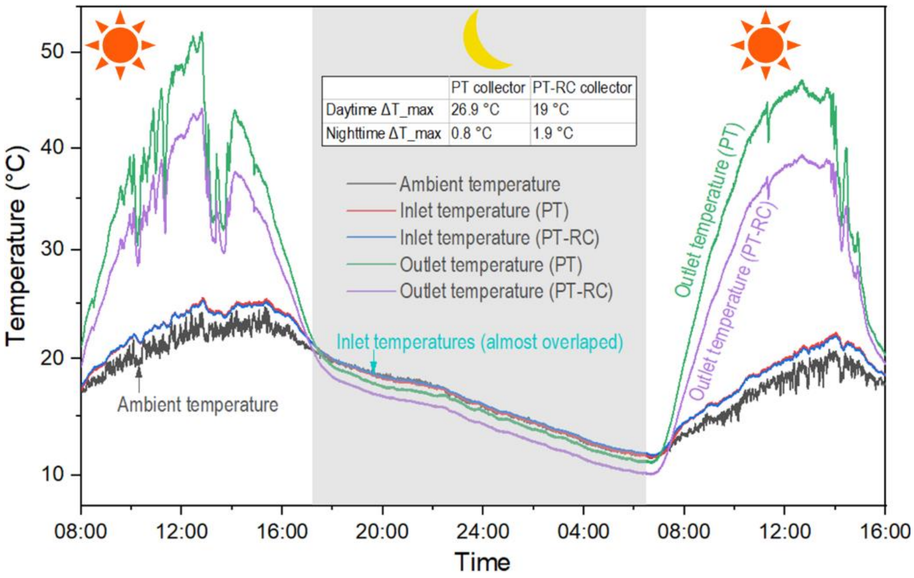

Fig. 4. Temperature profiles of the PT and PT-RC collectors over 32-hour consecutive testing. Note: offset reciprocal is applied on the vertical axis.

Although its diurnal solar heating performance deteriorates, the PT-RC collector shows better nocturnal radiative cooling capacity than the PT collector. The PT collector was not designed for radiative cooling and thus its cooling performance during the radiative cooling mode (18:00 to 6:30) was negligible, with the maximum inlet-outlet air temperature difference being 0.8 °C and the average cooling power being 10.0 W/m^2. In contrast, the PT-RC collector had a maximum inlet-outlet air temperature difference of 1.9 °C and an average cooling power of 30.3 W/m^2. Unlike its effect during the daytime solar heating mode, the PE film contributes to the cooling performance enhancement of the PT-RC collector during the nighttime radiative cooling mode. This is because the PE film atop the glass cover of the PT-RC collector significantly decreases the convection heat exchange between the warm ambient air and cold glass cover in this scenario, enabling the glass cover to reach a lower temperature and cool the beneath air stream more effectively. In contrast, the glass cover of the PT collector directly contacts with the ambient air and thus cannot cool itself to a significant sub-ambient temperature. Moreover, the airflow in the PT collector does not directly exchange heat with the glass cover but with the solar absorber, which further decreases the inlet-outlet air temperature reduction. Considering that the PT-RC collector can provide energy in daytime and nighttime and match the energy demands in different seasons better, a small concession in solar heating performance is deemed acceptable when applied in four-season or tropical regions where cooling is unavoidable.

Table 2. Performance of the PT and PT-RC collectors from 08:00, Nov 2nd to 16:00, Nov 3rd, 2020. (Average values are listed)

Period	$\bar{T}_{a}$ (°C)	$\bar{T}_{in\_PT}$ (°C)	$\bar{T}_{in\_PT-RC}$ (°C)	$\bar{T}_{out\_PT}$ (°C)	$\bar{T}_{out\_PT-RC}$ (°C)	$\bar{\eta}_{th\_PT}$ (%)	$\bar{\eta}_{th\_PT-RC}$ (%)	$\bar{P}_{co\_PT}$ (W/m^2)	$\bar{P}_{co\_PT-RC}$ (W/m^2)
08:00 to 16:00 (Nov 2nd)	21.3	23.0	22.9	37.9	33.3	47.4 ± 3.1	32.8 ± 3.5	/	/
18:00 to 06:30	15.6	15.6	15.8	15.1	14.1	/	/	10.0 ± 1.6	30.3 ± 1.6
08:00 to 16:00 (Nov 3rd)	17.4	19.0	18.9	36.2	31.0	47.5 ± 3.1	33.4 ± 3.6	/	/

4.2. Effect of inlet air temperature

In practical situations, the inlet air temperature of a PT-RC collector is not necessarily equal or close to that of the ambient air. For example, the inlet of the collector may be fed by air from a building or a preceding PT-RC collector. Therefore, the performance of the PT-RC collector under different inlet-ambient temperature differences is discussed in this section.

Firstly, the influence of the inlet-ambient temperature gap on the solar heating performance was tested around noon-time on November 8th, 2020, during which the solar irradiance and ambient temperature were relatively stable, as shown in Fig. 5. The mass flow rate of the air stream in the two collectors was stabilized at about 0.03 kg/s during the test. By gradually increasing the heating power in the air handling unit, the inlet air temperature was lifted stepwise from a level slightly higher than the ambient temperature (about 22 °C) to around 36 °C. Fig. 5 also illustrates the outlet temperature profiles of the PT and PT-RC collectors against different inlet temperatures. It is worth pointing out that, to minimize the interference of state-transition to test accuracy, only the data recorded in the last three minutes of each step were selected for performance analysis. Not surprisingly, the outlet temperature in the PT-RC collector is lower than that in the PT collector, reflecting the difference between the two collectors in solar heating capacity.

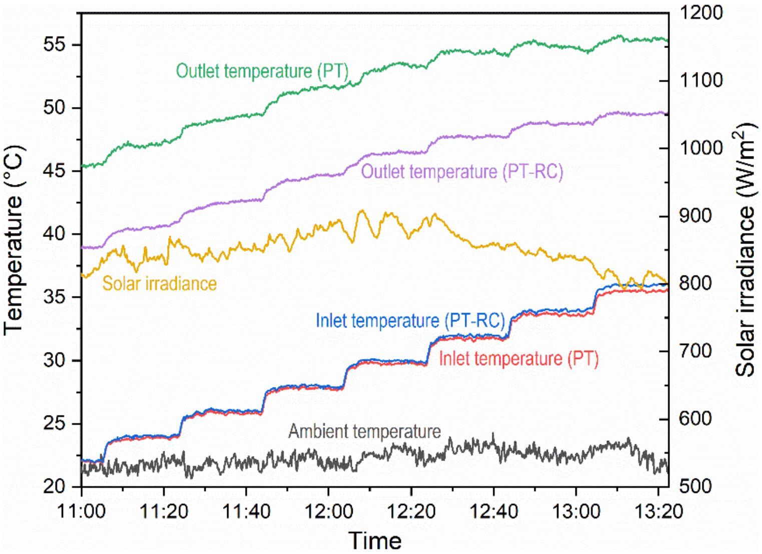

Fig. 5. The inlet and outlet temperature profiles of the PT and PT-RC collectors and the weather data during the solar heating mode with different inlet-ambient temperature differences.

By extracting the valid testing data, the solar thermal efficiency of the two collectors under different inlet temperatures can be obtained. To eliminate the effect of solar irradiance variation and temperature difference between the ambient air and inlet air and to obtain general conclusions, a term named reduced temperature is employed for discussion, which is defined as the temperature increment of the inlet air relative to the ambient air divided by the solar irradiance, expressed as $(T_{in}-T_a)/G$ [38]. Fig. 6 shows the thermal efficiency of the two collectors at different reduced temperatures. Generally, the thermal efficiency decreases linearly at increased reduced temperatures due to the increased thermal loss of the collector. Through linear regression on the data set in Fig. 6, the thermal efficiency of the PT and PT-RC collectors can be expressed as follows (with three significant digits):

$$\eta_{\text{th\_PT}}\Big|_{\dot{m}=0.03\text{kg/s}} = 0.474 - 4.25\frac{T_{\text{in}} - T_{\text{a}}}{G} \tag{8}$$

$$\eta_{\text{th\_PT-RC}}\Big|_{\dot{m}=0.03\text{kg/s}} = 0.34.2 - 3.73\frac{T_{\text{in}} - T_{\text{a}}}{G} \tag{9}$$

in which the intercepts 0.474 and 0.342 are the thermal efficiency of the two collectors at zero-reduced temperature; and the slopes −4.25 and −3.73 are the thermal loss coefficient of the two collectors in the solar heating mode, K·m^2/W. As suggested from Eqs. (8) and (9), the thermal efficiency of the PT-RC collector is about 72.2% of that of the PT collector at zero-reduced temperature. However, considering that the thermal loss coefficient of the PT-RC collector is smaller than that of the PT collector, the PT-RC collector will show closer thermal efficiency to the PT collector at higher $(T_{\text{in}}-T_{\text{a}})/G$, which is a common situation in real-world applications. Besides, the *MRE* of the thermal efficiency of the PT and PT-RC collectors are very low, with the value being 2.7% and 3.0%, respectively.

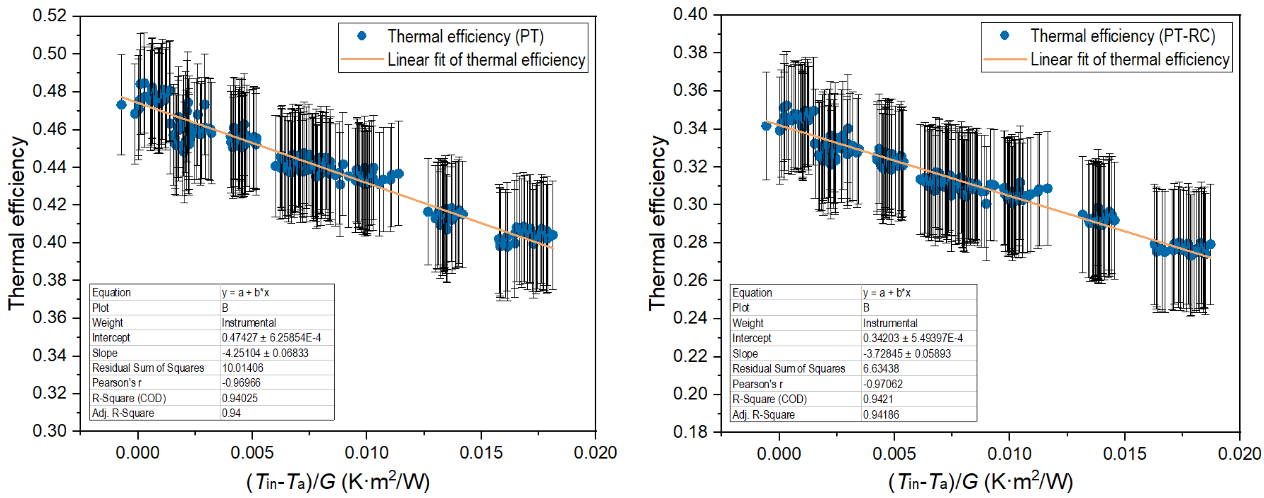

Fig. 6. The thermal efficiency of the typical PT collector and air-based PT-RC collector at different reduced temperatures.

Soon after the solar heating performance testing, the effect of the inlet-ambient temperature difference on the radiative cooling performance was tested from 22:00 November 8$^{\text{th}}$ to 05:00 November 9$^{\text{th}}$, 2020. The air mass flow rates of the two collectors were also kept at about 0.03 kg/s during the test. As the ambient temperature during the night usually decreases gradually, we stabilized the inlet temperature at about 14.1°C to create a series of inlet-ambient temperature differences ($T_{in}-T_a$), as shown in Fig. 7. Overall, the temperature reduction of the air stream passing through the two collectors increases at elevated ($T_{in}-T_a$). Two equations of linear regression can be derived from the data set illustrated in Fig. 8, expressed as follows (with three significant digits):

$$P_{co\_PT}\Big|_{\dot{m}=0.03\text{kg/s}} = 11.4 + 2.17\left(T_{in} - T_a\right) \tag{10}$$

$$P_{co\_PT\text{-}RC}\Big|_{\dot{m}=0.03\text{kg/s}} = 27.9 + 2.18\left(T_{in} - T_a\right) \tag{11}$$

where the intercepts 11.4 and 27.9 are the net radiative cooling power (e.g., when the inlet air temperature equals the ambient temperature) of the two collectors, W/m^2; and the slopes 2.17 and 2.18 are the thermal loss coefficient of the two collectors in the radiative cooling mode, W/(m^2·K). As indicated in Eqs. (10) and (11), the net radiative cooling power of the PT-RC collector is about 2.4 times that of the PT collector. Considering that the thermal loss coefficient of the two collectors are almost the same, the PT-RC collector will always show higher cooling power than the PT collector in sub-ambient conditions. In addition, the *MRE* of the cooling power of the PT collector is relatively high, with the value being 14.8%, which is mainly because of the small inlet-outlet air temperature difference. In contrast, the *MRE* of the cooling power of the PT-RC collector is much lower, with the value being 5.5%. Besides, similar to the fact that an air-based solar collector is inferior to a water-based one in thermal efficiency [39], the proposed air-based PT-RC collector shows lower cooling capacity compared to the water-based PT-RC collector [31].

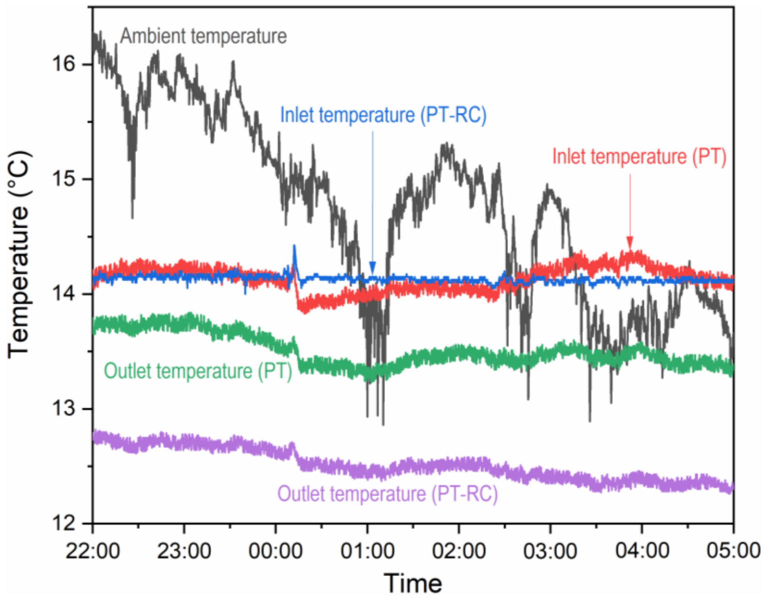

Fig. 7. The inlet and outlet temperature profiles of the PT and PT-RC collectors and the weather data during the radiative cooling mode with different inlet-ambient temperature differences.

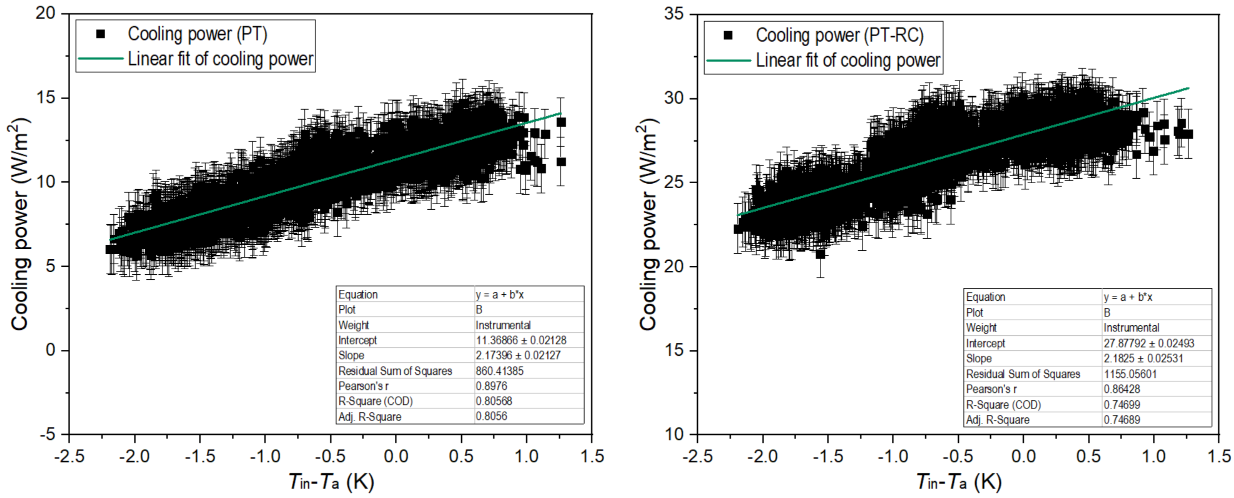

Fig. 8. The cooling power of the typical PT collector and air-based PT-RC collector at different inlet-ambient air temperature differences.

4.3. Effect of mass flow rate

The air mass flow rate of the PT-RC collector may vary in different practical application scenarios. Therefore, the influence of air mass flow rate on the solar heating and radiative cooling performance of the PT-RC collector is investigated and compared with that of the PT collector in this section. The experiment was carried out on four consecutive days (from November 10th to 13th, 2020) with quite similar weather conditions indicated in Table 3. The mass flow rate of the air stream in the two collectors was set at 0.03, 0.05, and 0.01 kg/s (corresponding to an air velocity of about 0.80, 1.34, 0.27 m/s, respectively in the air duct) in sequence during the test.

Table 3. Weather data on November 10th, 11th, 12th, and 13th, 2020.

Parameter		Nov. 10th to 11th ($\dot{m} \approx 0.03$kg/s)	Nov. 11th to 12th ($\dot{m} \approx 0.05$kg/s)	Nov. 12th to 13th ($\dot{m} \approx 0.01$kg/s)
Average solar irradiance (W/m^2)	09:00 to 15:00	728.9	777.9	760.5
	22:00 to 06:00	0	0	0
Average ambient temperature (°C)	09:00 to 15:00	19.5	19.4	19.7
	22:00 to 06:00	13.7	13.7	13.6
Average wind velocity (m/s)	09:00 to 15:00	1.6	1.9	1.1
	22:00 to 06:00	0.8	0.9	0.2

Fig. 9 compares the thermal efficiency of the PT and PT-RC collectors during the solar heating mode with different air mass flow rates. Testing results indicate that the thermal efficiency increases at increased mass flow rates for both collectors, which is mainly due to the greater heat transfer coefficient at lifted mass flow rates. Besides, a higher mass flow rate corresponds to a lower outlet temperature and thus a lower average air temperature in the air duct, which means less heat is dissipated from the air stream to the ambient through the collector, further increasing the thermal efficiency in this case. However, the thermal efficiency tends to be less sensitive to the air mass flow rate as the latter increases, which is in line with the findings reported in other studies [40, 41]. Table 4 details the thermal performance of the two collectors during the solar heating mode test. As the air mass flow rate increases from 0.01 to 0.05 kg/s, the thermal efficiency of the PT collector surges from 25.3% to 45.7%, and that of the PT-RC collector elevates from 19.8% to 34.5%. However, the increment of mass flow rate from 0.03 to 0.05kg/s only results in efficiency gains of 1.1 and 2.1 percent points for the two collectors, respectively. Besides, as the increase of the air mass flow rate, the *MRE* of the thermal efficiency of the two collectors increases slightly, which results from the decrement of inlet-outlet air temperature difference.

Fig. 10 presents the cooling power of the two collectors during the radiative cooling mode with different air mass flow rates. A higher mass flow rate corresponds to greater heat exchange between the glass cover and air stream and thus facilitates the increment in cooling power for the PT-RC collector, but this facilitation becomes weaker as the mass flow rate increases from 0.03 to 0.05kg/s. For the PT collector, the cooling power curves for the two mass flow rates even overlap at most time during the test, indicating that the influence of air mass flow rate exceeding 0.03 kg/s on its cooling performance is negligible. Table 4 also lists some key experimental data of the two collectors during the radiative cooling mode test. The PT-RC collector nearly doubles its cooling power (from 16.9 to 33.0 W/m^2) as the mass flow rate lifts from 0.01 to 0.05kg/s. However, due to its insufficient radiative cooling capacity, the PT collector is barely sensitive to the change in mass flow rate. Its cooling power even saw a slight decrement from 11.2 to 11.0 W/m^2 as the mass flow rate increased from 0.03 to 0.05kg/s during the experiment. This is probably because the weather condition was more unfavorable to radiative cooling on that night (November 11st to 12nd) with a mass flow rate of 0.05kg/s, and this adverse impact overwhelmed the benefit resulting from mass flow rate increment. Besides, different from the slight variation of the *MRE* of the thermal efficiency of the two collectors at different air mass flow rates, the *MRE* of the cooling power varies remarkably as the air mass flow rate increases from 0.01 to 0.05 kg/s, which results from the relatively small inlet-outlet temperature difference in the radiative cooling mode. For instance, the *MRE* of the cooling power of the PT-RC collector is 2.9% when the air mass flow rate is 0.01 kg/s, and it increases to 6.8% when the latter increases to 0.05%.

In addition, it is worth pointing out that the increase in thermal efficiency and cooling power are obtained at the cost of the increase in electrical energy consumption of the air blower. Therefore, considering the gradually declined increasing rate of thermal efficiency and cooling power but gradually augmented on-way resistance at increased air mass flow rate, the rise in air mass flow rate will not always result in the increment of systematic heating and cooling performance. A limitation of the experiment is that the pressure drops of the air stream when passing through the two collectors under different mass flow rates were not measured. This pressure drop data would help to better reflect the relationship between the performance of the collector and the air mass flow rate.

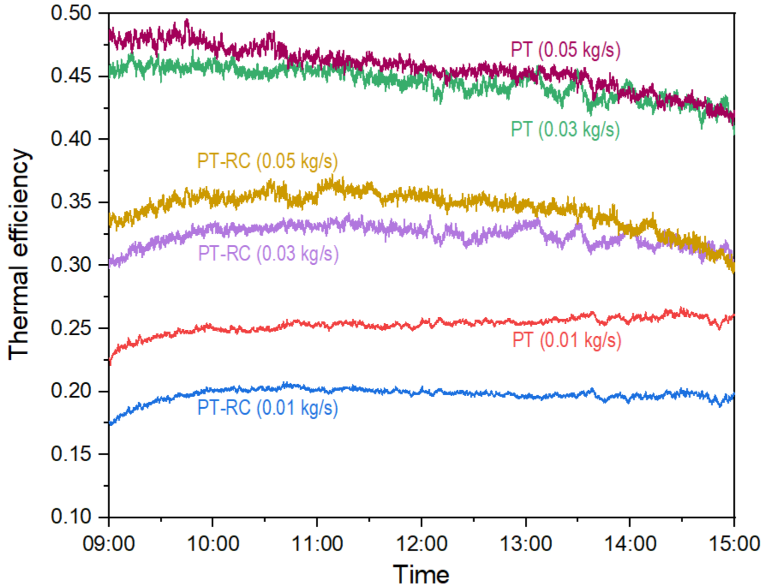

Fig. 9. The thermal efficiency of the PT and PT-RC collectors during the solar heating mode with different air mass flow rates. Note: For the PT collector, the relative mean error of the thermal efficiency is 2.5%, 2.7%, and 3.0% when the air mass flow rate is 0.01 kg/s, 0.03kg/s, and 0.05 kg/s, respectively; For the PT-RC collector, the relative mean error of the thermal efficiency is 2.6%, 2.9%, and 3.2% when the air mass flow rate is 0.01 kg/s, 0.03kg/s, and 0.05 kg/s, respectively

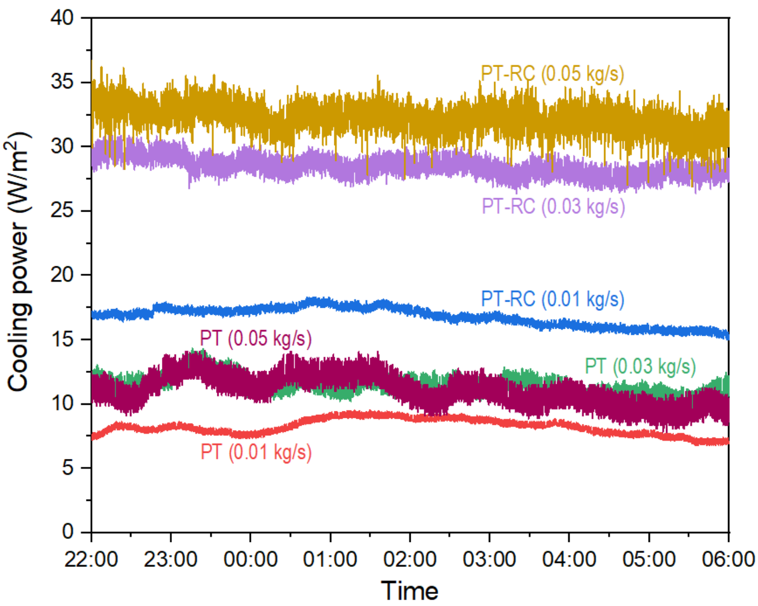

Fig. 10. The cooling power of the PT and PT-RC collectors during the radiative cooling mode with different air mass flow rates. Note: For the PT collector, the relative mean error of the cooling power is 6.0%, 12.0%, and 22.9% when the air mass flow rate is 0.01 kg/s, 0.03kg/s, and 0.05 kg/s, respectively; For the PT-RC collector, the relative mean error of the cooling power is 2.9%, 5.0%, and 6.8% when the air mass flow rate is 0.01 kg/s, 0.03kg/s, and 0.05 kg/s, respectively

Table 4. Performance of the PT and PT-RC collectors against different air mass flow rates. (Average values are listed)

Mass flow rate (kg/s)		$\overline{T}_a$ (°C)	$\overline{T}_{in\_PT}$ (°C)	$\overline{T}_{in\_PT\text{-}RC}$ (°C)	$\overline{T}_{out\_PT}$ (°C)	$\overline{T}_{out\_PT\text{-}RC}$ (°C)	$\overline{\eta}_{th\_PT}$ (%)	$\overline{\eta}_{th\_PT\text{-}RC}$ (%)	$\overline{P}_{co\_PT}$ (W/m^2)	$\overline{P}_{co\_PT\text{-}RC}$ (W/m^2)
Solar heating mode	0.01	19.7	23.3	23.2	61.9	53.2	25.3 ± 2.5	19.8 ± 2.6	/	/
	0.03	19.5	21.0	21.0	41.1	35.6	44.6 ± 2.7	32.4 ± 2.9	/	/
	0.05	19.4	20.7	20.7	34.8	31.4	45.7 ± 3.0	34.5 ± 3.2	/	/
Radiative cooling mode	0.01	13.6	15.0	15.1	13.5	12.0	/	/	8.0 ± 0.5	16.9 ± 0.5
	0.03	13.7	14.3	14.4	13.7	12.7	/	/	11.0 ± 1.5	28.6 ± 1.5
	0.05	13.7	14.3	14.5	13.9	13.2	/	/	10.8 ± 2.3	33.0 ± 2.3

5. Conclusions

In this study, an idea of extending the operation of the flat-plate solar air collector to night-time by incorporating radiative sky cooling is proposed. A new dual-mode collector, named as air-based solar photothermic and radiative cooling (PT-RC) collector, is designed, constructed, and experimentally investigated along with a typical flat-plate air-based solar collector. The experimental research helps to draw the following conclusions:

(1) The proposed PT-RC collector successfully demonstrated a favorable daytime solar heating and nighttime radiative cooling capacity, while the typical solar collector showed negligible productivity at night.

(2) During a consecutive 32-hour test with near-ambient inlet air temperatures and a mass flow rate of around 0.03kg/s, the PT-RC collector showed an average thermal efficiency of 33.1% during the solar heating period (08:00 to 16:00) and an average cooling power of 30.3 W/m^2, which are respectively 70% and three times of those of the typical solar air collector.

(3) Investigation on the effect of inlet air temperature on the thermal performance suggested that, with a mass flow rate of 0.03kg/s, the thermal efficiency of the PT-RC collector was 34.2% at zero-reduced temperature, and the net radiative cooling power reached 27.9 W/m^2.

(4) Increasing the air mass flow rate can augment both the solar thermal efficiency and cooling capacity of the PT-RC collector. As the mass flow rate increased from 0.01 to 0.05kg/s, the two performance indicators of the PT-RC collector lifted from 19.8% to 34.5% and from 16.9 to 33.0 W/m^2, respectively.

On the whole, this study proposed a new way to integrate solar energy harvesting and radiative cooling into a single system to overcome the limitations of stand-alone solar collectors and radiative coolers in terms of operation continuity, flexibility, and efficacy. Although showing worse solar heating performance compared with the typical solar air collector, the air-based PT-RC collector can work day and night continuously and has better seasonal and regional adaptability, making it more practical when applied in four-season regions where heating and cooling are both required throughout the year or tropical zones where cooling is much demanded. This study may also help to identify new research topics in the area of solar energy, radiative cooling, building energy-saving, etc. As the thermal performance of the proposed air-based PT-RC collector is relatively worse than the water-based PT-RC collector, further studies should pay attention to augmenting the heat transfer coefficient between the air stream and the panels by such strategies as adding roughness structures and double-pass arrangement, etc. In addition, as the PE cover used in the PT-RC collector is fragile and will show degraded transmissivity after long-term exposure to sunlight, another future emphasis would be developing an alternative cover with better durability for wider real-world applications.

Acknowledgments

This study was sponsored by the H2020 Marie Skłodowska-Curie Actions - Individual Fellowships (842096), National Natural Science Foundation of China (NSFC 51906241, 51776193, and 52106276), and Anhui Provincial Natural Science Foundation (1908085ME138 and 2008085QE234).

Nomenclature

A	Area, m^2
C	Flow coefficient, -
c	Specific heat capacity, J/(kg·K)
G	Solar irradiance, W/m^2
H	Total incident solar radiation, J/s
$\dot{m}$	Air mass flow rate, kg/s
P	Cooling power, W/m^2
p	Pressure, Pa
$\overline{P}$	Average cooling power, W/m^2
Q	Thermal energy gain, J/s
RE	Relative error, -
RME	Relative mean error, -

T	Temperature, K
$\overline{T}$	Average temperature, K
V' and V	Specific volume of the air, m^3/kg
W	Moisture content of the air, g/kg
η	Solar thermal efficiency, -
$\overline{\eta}$	Average solar thermal efficiency, -

Abbreviation and subscripts

a	Ambient air
c	Collector
co	Cooling
in	Collector inlet
n	Nozzle
out	Collector outlet
th	Thermal
w	Water

Data Availability

The data that support the findings of this study are available from the corresponding author upon reasonable request.

References

[1] Li X, Yao X. Can energy supply-side and demand-side policies for energy saving and emission reduction be synergistic?--- A simulated study on China's coal capacity cut and carbon tax. Energy Policy. 2020;138:111232.

[2] He F, Fathabadi H. Novel standalone plug-in hybrid electric vehicle charging station fed by solar energy in presence of a fuel cell system used as supporting power source. Renewable Energy. 2020;156:964-74.

[3] Thirugnanasambandam M, Iniyan S, Goic R. A review of solar thermal technologies. Renewable and sustainable energy reviews. 2010;14:312-22.

[4] Gautam A, Saini RP. A review on sensible heat based packed bed solar thermal energy storage system for low temperature applications. Solar Energy. 2020;207:937-56.

[5] Eterafi S, Gorjian S, Amidpour M. Thermodynamic design and parametric performance assessment of a novel cogeneration solar organic Rankine cycle system with stable output. Energy Conversion and Management. 2021;243:114333.

[6] Wang Q, Yang H, Zhong S, Huang Y, Hu M, Cao J, et al. Comprehensive experimental testing and analysis on parabolic trough solar receiver integrated with radiation shield. Applied Energy. 2020;268:115004.

[7] Yu G, Yu J, Hu Y, Cheng X, Liu H, Liu W. Moisture transport analysis for integrated structures of flat plate solar collector and building envelope. Solar Energy. 2021;217:145-54.

[8] Kamarulzaman A, Hasanuzzaman M, Rahim NA. Global advancement of solar drying technologies and its future prospects: A review. Solar Energy. 2021;221:559-82.

[9] Olkis C, Al-Hasni S, Brandani S, Vasta S, Santori G. Solar powered adsorption desalination for Northern and Southern

Europe. Energy. 2021;232:120942.
[10] Yang M, Wang Z, Chen L, Tang W. Dynamic heat transfer model of flat plate solar water collectors with consideration of variable flow rate. Solar Energy. 2020;212:34-47.
[11] Qasem NAA, Arnous MN, Zubair SM. A comprehensive thermal-hydraulic assessment of solar flat-plate air heaters. Energy Conversion and Management. 2020;215:112922.
[12] Dezan DJ, Rocha AD, Ferreira WG. Parametric sensitivity analysis and optimisation of a solar air heater with multiple rows of longitudinal vortex generators. Applied Energy. 2020;263:114556.
[13] Benhamza A, Boubekri A, Atia A, El Ferouali H, Hadibi T, Arıcı M, et al. Multi-objective design optimization of solar air heater for food drying based on energy, exergy and improvement potential. Renewable Energy. 2021;169:1190-209.
[14] Wang Z, Diao Y, Zhao Y, Wang T, Liang L, Chi Y. Experimental investigation of an integrated collector–storage solar air heater based on the lap joint-type flat micro-heat pipe arrays. Energy. 2018;160:924-39.
[15] Al-damook A, Khalil WH. Experimental evaluation of an unglazed solar air collector for building space heating in Iraq. Renewable Energy. 2017;112:498-509.
[16] Fudholi A, Sopian K. A review of solar air flat plate collector for drying application. Renewable and Sustainable Energy Reviews. 2019;102:333-45.
[17] Xiao H, Dong Z, Liu Z, Liu W. Heat transfer performance and flow characteristics of solar air heaters with inclined trapezoidal vortex generators. Applied Thermal Engineering. 2020;179:115484.
[18] Pelenovich V, Liu H, Zeng X, Liu Y, Liu K, Yang B. Graded solar selective absorbers deposited by non-equilibrium RF magnetron sputtering. Solar Energy Materials and Solar Cells. 2021;230:111188.
[19] Hu M, Zhao B, Ao X, Su Y, Pei G. Parametric analysis and annual performance evaluation of an air-based integrated solar heating and radiative cooling collector. Energy. 2018;165:811-24.
[20] Hu Z, He W, Hong X, Ji J, Shen Z. Numerical analysis on the cooling performance of a ventilated Trombe wall combined with venetian blinds in an office building. Energy and Buildings. 2016;126:14-27.
[21] Singh AP, Kumar A, Akshayveer, Singh OP. Effect of integrating high flow naturally driven dual solar air heaters with Trombe wall. Energy Conversion and Management. 2021;249:114861.
[22] Hu M, Zhao B, Ao X, Suhendri, Cao J, Wang Q, et al. Performance analysis of a novel bifacial solar photothermic and radiative cooling module. Energy Conversion and Management. 2021;236.
[23] Zhao D, Aili A, Zhai Y, Xu S, Tan G, Yin X, et al. Radiative sky cooling: Fundamental principles, materials, and applications. Applied Physics Reviews. 2019;6.
[24] Hu M, Suhendri, Zhao B, Ao X, Cao J, Wang Q, et al. Effect of the spectrally selective features of the cover and emitter combination on radiative cooling performance. Energy and Built Environment. 2021;2:251-9.
[25] Chae D, Kim M, Jung P-H, Son S, Seo J, Liu Y, et al. Spectrally selective inorganic-based multilayer emitter for daytime radiative cooling. ACS applied materials & interfaces. 2020;12:8073-81.
[26] Li D, Liu X, Li W, Lin Z, Zhu B, Li Z, et al. Scalable and hierarchically designed polymer film as a selective thermal emitter for high-performance all-day radiative cooling. Nature Nanotechnology. 2021;16:153-8.
[27] Huang Z, Ruan X. Nanoparticle embedded double-layer coating for daytime radiative cooling. International Journal of Heat and Mass Transfer. 2017;104:890-6.
[28] Hu M, Zhao B, Ao X, Feng J, Cao J, Su Y, et al. Experimental study on a hybrid photo-thermal and radiative cooling collector using black acrylic paint as the panel coating. Renewable Energy. 2019;139:1217-26.
[29] Gentle AR, Smith GB. Is enhanced radiative cooling of solar cell modules worth pursuing? Solar Energy Materials and Solar Cells. 2016;150:39-42.
[30] Matsuta M, Terada S, Ito H. Solar heating and radiative cooling using a solar collector-sky radiator with a spectrally selective surface. Solar Energy. 1987;39:183-6.
[31] Hu M, Pei G, Wang Q, Li J, Wang Y, Ji J. Field test and preliminary analysis of a combined diurnal solar heating and

nocturnal radiative cooling system. Applied Energy. 2016;179:899-908.
[32] Zhao B, Ao X, Chen N, Xuan Q, Hu M, Pei G. A spectrally selective surface structure for combined photo-thermic conversion and radiative sky cooling. Frontiers in Energy. 2020.
[33] Liu J, Zhou Z, Zhang D, Jiao S, Zhang J, Gao F, et al. Research on the performance of radiative cooling and solar heating coupling module to direct control indoor temperature. Energy Conversion and Management. 2020;205:112395.
[34] Hu M, Zhao B, Suhendri S, Cao J, Wang Q, Riffat S, et al. Experimental study on a hybrid solar photothermic and radiative cooling collector equipped with a rotatable absorber/emitter plate. Applied Energy. 2022;306.
[35] Li X, Sun B, Sui C, Nandi A, Fang H, Peng Y, et al. Integration of daytime radiative cooling and solar heating for year-round energy saving in buildings. Nature Communications. 2020;11:6101.
[36] Ramani BM, Gupta A, Kumar R. Performance of a double pass solar air collector. Solar Energy. 2010;84:1929-37.
[37] Hegazy AA. Comparative study of the performances of four photovoltaic/thermal solar air collectors. Energy Conversion and management. 2000;41:861-81.
[38] Duffie JA, Beckman WA. Solar engineering of thermal processes: John Wiley & Sons; 2013.
[39] Wang D, Liu J, Liu Y, Wang Y, Li B, Liu J. Evaluation of the performance of an improved solar air heater with “S” shaped ribs with gap. Solar Energy. 2020;195:89-101.
[40] Ma J, Sun W, Ji J, Zhang Y, Zhang A, Fan W. Experimental and theoretical study of the efficiency of a dual-function solar collector. Applied Thermal Engineering. 2011;31:1751-6.
[41] Dong Z, Chang L, Jianjun Z, Jinlong J, Zhoujian A, Linjun W. Thermal economic analysis of a double-channel solar air collector coupled with draught fan: Based on energy grade. Renewable Energy. 2021;170:936-47.

Declaration of interests

☑The authors declare that they have no known competing financial interests or personal relationships that could have appeared to influence the work reported in this paper.

☐The authors declare the following financial interests/personal relationships which may be considered as potential competing interests:

- Mingke Hu: Conceptualization, Methodology, Formal analysis, Investigation, Funding acquisition, Writing - Original Draft, Writing - Review & Editing
- Bin Zhao: Methodology, Formal analysis, Investigation
- Suhendri: Formal analysis, Writing - Review & Editing
- Jingyu Cao: Formal analysis, Investigation
- Qiliang Wang: Formal analysis, Writing - Review & Editing
- Saffa Riffat: Resources, Project administration, Supervision
- Yuehong Su: Supervision, Project administration, Funding acquisition, Writing - Review & Editing
- Gang Pei: Conceptualization, Resources, Supervision, Project administration, Funding acquisition, Writing - Review & Editing